JOURNAL OF MAGNETIC RESONANCE **126,** 58–65 (1997)
ARTICLE NO. MN971159

Longitudinal Relaxation and Diffusion Measurements Using Magnetic Resonance Signals from Laser-Hyperpolarized ^{129}Xe Nuclei

Baldev R. Patyal,* Jia-Hong Gao,*,† Robert F. Williams,* John Roby,* Brian Saam,‡ Benjamin A. Rockwell,§ Robert J. Thomas,§ David J. Stolarski,¶ and Peter T. Fox*

*Research Imaging Center, University of Texas Health Science Center, San Antonio, Texas 78284; ‡Department of Physics, Princeton University, Princeton, New Jersey 08544; §Armstrong Laboratory, Brooks Air Force Base, San Antonio, Texas 78235; and ¶The Analytic Sciences Corp., San Antonio, Texas 78212

Received September 23, 1996; revised March 5, 1997

Methods for T_1 relaxation and diffusion measurements based on magnetic resonance signals from laser-hyperpolarized ^{129}Xe nuclei are introduced. The methods involve optimum use of the perishable hyperpolarized magnetization of ^{129}Xe. The necessary theoretical framework for the methods is developed, and then the methods are applied to measure the longitudinal relaxation constant, T_1, and the self-diffusion constant, D, of hyperpolarized ^{129}Xe. In a cell containing natural abundance ^{129}Xe at 790 Torr, the T_1 value was determined to be 155 ± 5 min at 20°C and at 2.0 T field. For a second cell at 896 Torr, at the same field and temperature, the T_1 value was determined to be 66 ± 2 min. At a higher field of 7.05 T, the T_1 values for the two cells were found to be 185 ± 10 and 88 ± 5 min, respectively. The ^{129}Xe self-diffusion constant for the first cell was measured to be 0.057 cm^2/s and for the second cell it was 0.044 cm^2/s. The methods were applied to ^{129}Xe in the gas phase, *in vitro;* however, they are, in principle, applicable for *in vivo* or *ex vivo* studies. The potential role of these methods in the development of newly emerging hyperpolarized ^{129}Xe MRI applications is discussed.

INTRODUCTION

Recent developments in MRI using laser-polarized ^{129}Xe (*1*) and ^{3}He (*2*) have generated a great deal of interest in their potential applications in imaging of human lungs, brain, blood vessels, and other structures. Hyperpolarized ^{3}He, due to its low solubility in blood and tissue, is primarily suitable for imaging air spaces, whereas ^{129}Xe holds great promise for imaging of brain and other tissue (*1, 2*). The major obstacles in using ^{129}Xe as a magnetic resonance signal source in conventional MRI are its low sensitivity (0.02 that of ^{1}H) and its low achievable concentration in tissue (≈10 m*M* as compared to 80–100 *M* ^{1}H concentration in ^{1}H MRI) (*1, 3*). What makes MRI feasible with ^{129}Xe is the capability to produce ^{129}Xe nuclear spin polarizations that are 10^5–10^6 higher than those obtained in conventional thermal equilibrium NMR experiments. This tremendous increase in the ^{129}Xe nuclear spin polarization nearly compensates for the reduced sensitivity and lower concentration of ^{129}Xe in tissue compared to ^{1}H. This hyperpolarization is achieved through collisional spin exchange of ^{129}Xe nuclei with Rb atoms optically pumped and polarized with circularly polarized 795 nm laser light (*4–6*).

Xenon once inhaled is rapidly transferred from lungs to blood and thence to tissue; consequently, the development of this technique as an imaging modality for brain, blood vessels, and other tissue is critically dependent upon whether the hyperpolarized ^{129}Xe retains its polarization sufficiently long to reach the tissue of interest. Since the hyperpolarized magnetization decays with the longitudinal relaxation constant, T_1, a knowledge of this parameter for ^{129}Xe in tissue is very important. T_1 for xenon has been measured in conventional thermal equilibrium ^{129}Xe NMR experiments, *in vitro* (*3, 7, 8*), and recently using hyperpolarized ^{29}Xe, *in vitro* (*9*) and *in vivo* (*10–12*).

A second mechanism for the loss of hyperpolarization is the so-called cos θ loss, where θ is the magnetization tilt angle introduced by the RF pulse. In conventional ^{1}H magnetic resonance, we are generally not concerned about this loss, because the magnetization is recovered to its thermal equilibrium value after the pulse. In this new magnetic resonance architecture, however, the RF tilt causes a permanent loss of hyperpolarized magnetization; e.g., after a 90° pulse, all the hyperpolarized magnetization is gone. Consequently, to design efficient pulse sequences based on hyperpolarized ^{129}Xe magnetic resonance, it is critical to make the most optimum use of the total available hyperpolarized magnetization, a ''use-it-or-lose-it'' strategy.

In this paper, we introduce methods for T_1 relaxation and ^{129}Xe diffusion measurements based on the magnetic resonance signal from hyperpolarized ^{129}Xe nuclei. Although demonstrated in the gas phase, *in vitro,* these methods can, in principle, be used for *in vivo* or *ex vivo* T_1 and ^{129}Xe-diffusion measurements. The methods involve optimum utilization of the perishable hyperpolarized magnetization of ^{129}Xe. Earlier, because of poor signal-to-noise ratio of the

† To whom correspondence should be addressed.

1090-7807/97 $25.00

^{129}Xe NMR signal at low pressures, diffusion measurements on ^{129}Xe using NMR were possible only at high pressures (*13*). Only recently, with hyperpolarized ^{129}Xe, diffusion measurements at low pressures using NMR have become possible (*14*).

The necessary theoretical framework for T_1 and diffusion measurements is developed first. The specific experiments to implement these methods and other pertinent experimental details are provided under Experimental. All the results are summarized in the section on results, and finally, the paper concludes with a discussion of the results and future applications of these methods.

THEORY

RF Pulse Width–Tip angle Calibration and T_1 Measurements

The ^{129}Xe self diffusion (D) and the longitudinal relaxation time (T_1) measurements, using hyperpolarized ^{129}Xe magnetic resonance, rely on an accurate calibration of the RF tip angle. Since the hyperpolarized nuclear magnetization, M_p, cannot be recovered by waiting for thermal equilibrium, we are faced with the task of designing new ways of performing spectroscopic and imaging experiments. The hyperpolarized nuclear spins lose their magnetization permanently by two mechanisms: (i) If left in a magnetic field, the hyperpolarized spins will proceed to their thermal equilibrium state with a relaxation constant T_1. (ii) When an RF pulse of tip angle, θ, is applied to the spin system in its hyperpolarized nonequilibrium state, the longitudinal magnetization, M_p, decreases by cos θ. Since $M_p \sim 10^5 M_0$, where M_0 is the thermal equilibrium magnetization, M_0 is negligible compared to M_p, and thus the residual longitudinal magnetization after n RF pulses, as a result of the relaxation mechanisms (i) and (ii), is (*15*)

$$M_z(n) = M_p \cos^n\theta e^{-(n-1)\mathrm{TR}/T_1} \quad [1]$$

and the corresponding signal intensity is

$$I(n) = M_y(n) \propto M_p \cos^{(n-1)}\theta \sin\theta\, e^{-(n-1)\mathrm{TR}/T_1}, \quad [2]$$

where TR is the pulse repetition time. Consequently, MR spectroscopy and MRI using hyperpolarized ^{129}Xe (or ^{3}He) require an optimization of the tip angle, θ, in order to preserve the precious but perishable hyperpolarized magnetization without losing a significant amount to T_1 relaxation. In order to calibrate the RF pulse and to determine the longitudinal relaxation time T_1, we developed two methods:

Method (a). First we developed a simple three pulse sequence θ—2θ—θ. The signal intensity after each pulse in this sequence can be written (Eq. [2]) as

$$I_1 \propto M_p \sin\theta \quad [3]$$

$$I_2 \propto M_p \cos\theta \sin 2\theta e^{-\mathrm{TR}/T_1} \quad [4]$$

$$I_3 \propto M_p \cos\theta \cos 2\theta \sin\theta e^{-2\mathrm{TR}/T_1}. \quad [5]$$

These three equations can be combined to give

$$\frac{I_2^2}{I_1 I_3} = \frac{4\cos^3\theta}{2\cos^2\theta - 1}. \quad [6]$$

Since I_1, I_2, and I_3 are experimentally measured quantities, and there is no T_1 dependence, θ can be directly calculated from Eq. [6].

Since θ is an unknown, an arbitrary RF pulse width can be set and θ can be calculated by solving the cubic in cos θ in Eq. [6]. A 90° RF pulse will consume all the hyperpolarized magnetization, which means I_2, $I_3 = 0$; on the other hand, a very small pulse width (very small θ) will result in very small signal-to-noise ratio, leading to larger errors in the determination of θ. Consequently, the optimum choice of initial pulse width to measure θ is an iterative process. In addition, although determination of θ through Eq. [6] is independent of T_1, TR must be small (TR $\ll T_1$) so that signal loss due to decay of ^{129}Xe hyperpolarized magnetization as a result of T_1 relaxation is minimized. Since there is no need to wait for thermal equilibrium to be established, TR can be chosen much shorter than T_1 and is in fact limited only by T_2^* and the data-acquisition time of the computer, both of which can be readily evaluated. We must add that the RF tip angle can also be changed by varying the pulse amplitude or RF power. This may be a method of choice to change RF tip angle for imaging *in vivo* where soft RF pulses must be used to select a given slice. The flip angle for a soft pulse is related to the pulse width in a nonlinear way, and the pulse width may be large.

Once θ is known, T_1 can be calculated from Eqs. [3]–[5]; however, TR is now set approximately T_1 to allow enough time for T_1 decay to occur. Also RF pulses should not be so wide that they become significant cause of decay. Because T_1 is the unknown, an educated guess must be made to set TR initially, and the experiment must then be repeated after choosing a more optimum value of TR to measure T_1.

Method (b). We developed a second method to determine the tip angle and also the longitudinal relaxation time T_1. It involves performing two sets of experiments. The first set measures the RF tip angle and the second set measures the relaxation time, T_1. To measure the RF tip angle, θ, a pulse train of 5 to 10 identical pulses, with very short TR (TR $\ll T_1$) between successive pulses, is applied.

The signal intensity after each pulse is given by Eq. [2]; consequently we can write

$$\frac{I(n)}{I(n-1)} = \cos\theta e^{-\mathrm{TR}/T_1} \approx \cos\theta,\ TR \ll T_1. \quad [7]$$

For example, if TR $\sim$ 1 s, $T_1 >$ 30 min, as was the case in our experiments, $e^{-1/1800} = 0.999$, the above approximation is indeed very well satisfied. Once the pulse width is

calibrated, a second set of experiments, with a pulse train of 4–5 RF pulses but with long TR (TR $\approx T_1$), can be performed. From the measured intensity of the signal after each pulse, T_1 can be calculated using ratios of adjacent signal intensities using Eq. [2]. The advantage of this method over the first is that in a single n-pulse sequence we get $n - 1$ measurements of θ, giving a more reliable measure of θ. In method (a), uncertainties in the measurement of intensities propagate into larger errors in the determination of θ from Eq. [6].

Diffusion Studies

Pulse optimization. The ^{129}Xe self-diffusion measurements reported in this paper are based on the optimum use of hyperpolarized magnetization of ^{129}Xe. If we apply the same RF pulse several times, the signal will decrease successively due to cos θ loss of the hyperpolarized magnetization even in the absence of T_1 depolarization which is not a desirable situation for performing imaging experiments. However, if TR is chosen to be much shorter than T_1, the tip angle θ for successive RF pulses can be manipulated to obtain a constant signal after each pulse. For the last pulse of such a sequence, a tip angle, $\theta = 90°$, will end all signal from the hyperpolarized magnetization ($\cos 90° = 0$). This formalism can be developed as follows:

Let $\theta_1, \theta_2, \ldots, \theta_n, \ldots, \theta_N$ be the tip angles for successive RF pulses. Let $Z_1, Z_2, \ldots, Z_n, \ldots, Z_N$ be the residual longitudinal magnetization after each pulse, and $X_1, X_2, \ldots, X_n, \ldots, X_N$ be the corresponding transverse magnetization. For negligible T_1 losses ($T_1 \gg$ TR), we can write

$$\begin{array}{lll} n & Z & X \\ 0 & Z_0 & 0 \\ 1 & Z_1 = Z_0\cos\theta_1 & X_1 = Z_0\sin\theta_1 \\ 2 & Z_2 = (Z_0\cos\theta_1)\cos\theta_2 & X_2 = (Z_0\cos\theta_1)\sin\theta_2 \\ & \quad = Z_1\cos\theta_2 & \quad = Z_1\sin\theta_2 \\ \cdots & & \\ n & Z_n = Z_{n-1}\cos\theta_n & X_n = Z_{n-1}\sin\theta_n. \end{array} \qquad [8]$$

It follows that

$$Z_n^2 + X_n^2 = Z_{n-1}^2. \qquad [9]$$

Now choose $\theta_1, \theta_2, \ldots, \theta_n$ such that $X_1 = X_2 = \ldots = X_n = X_c$ = constant. Using Eqs. [8] and [9], we can simplify

$$\frac{1}{\sin^2\theta_n} = \frac{Z_{n-1}^2}{X_c^2} = \frac{Z_n^2 + X_c^2}{X_c^2} = 1 + \frac{Z_n^2}{X_c^2}. \qquad [10]$$

Thus, for N such RF pulses, noting that the last pulse is constrained as $\theta_N = 90°$, and thereafter, $Z_N = 0$, Eq. [9] and Eq. [10] can be combined as a general expression for the tip angles θ_n to yield a constant signal

$$\frac{1}{\sin^2\theta_{N-n}} = N - n + 1, \qquad [11]$$

where N is the total number of RF pulses. For example, the design of a six-pulse experiment requires $N = 6$ with n varying from 1 to 6 as shown in Eq. [11]. Consequently, the tip angles, θ_n, of each successive pulse are calculated to result in equal signal intensity after each pulse. In situations where T_1 is very small, and TR $\sim T_1$, the T_1 decay should be included in the formalism as suggested for conventional ^{1}H snapshot FLASH (*16*), and recently for hyperpolarized ^{129}Xe magnetic resonance (*17*).

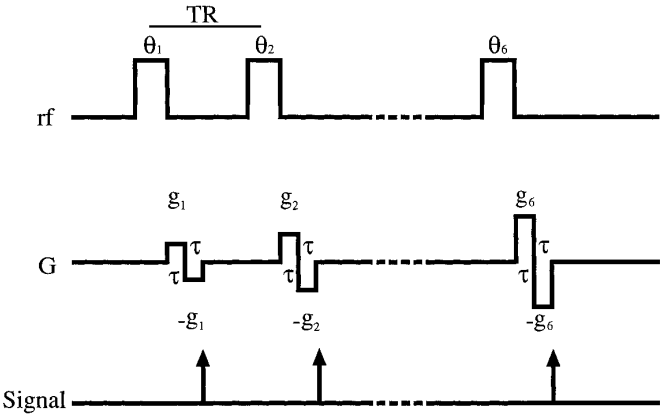

FIG. 1. Pulse sequence used for diffusion measurements. RF tilt angles, $\theta_1, \theta_2, \ldots, \theta_6$, and the corresponding pulse widths are listed in Table 1. The gradient duration, τ, was 9 ms. The gradient strengths $g_1, g_2, \ldots, g_6$ are also listed in Table 1.

Diffusion measurements. The pulse sequence used for diffusion measurements is shown in Fig. 1. It is the same pulse gradient sequence commonly used for NMR diffusion measurements (*18*) with one critical difference: the RF tip angles are varied from pulse to pulse according to the formalism developed in the previous section (Eq. [11]), so that in the absence of external gradients and negligible T_1 loss between pulses, the signal amplitude will remain constant after each pulse. The assumption of negligible T_1 relaxation between successive RF pulses is extremely well satisfied in our gas phase experiments, since TR $\sim$ 1 s, $T_1 >$ 30 min, resulting in only less than 0.05% loss in signal amplitude due to T_1 relaxation.

For the pulse sequence shown in Fig. 1, the signal after each pulse can be written as (*18*)

$$S_n = S_0 e^{-(2/3)\gamma^2 g_n^2 \tau^3 n D} = S_0 e^{-b_n D}, \qquad [12]$$

where S_0 is the signal in the absence of the gradient, S_n is the signal after the nth RF-gradient step, $b_n = \frac{2}{3}\gamma^2 g_n^2 \tau_n^3$, γ is the gyromagnetic ratio of the nucleus ($\gamma = 11.8$ MHz/T for ^{129}Xe), g_n is the gradient strength applied after the nth RF pulse, and τ_n is the gradient duration of the nth gradient. To change b_n linearly, we can manipulate the gradient duration, τ, and the gradient strength, g. Equation [12] can be rewritten as

$$\ln(S_n/S_0) = -b_n D. \qquad [13]$$

Thus from signal measurements after each RF-gradient step, we can calculate the diffusion constant, D, by a simple linear regression as shown in Eq. [13]. This method gives improved signal-to-noise ratio, especially at higher gradients, by providing higher transverse magnetization through tip angle optimization, consequently resulting in a better fit and better measurement of the diffusion constant.

EXPERIMENTAL

Sample Preparation

All experiments were performed on two Xe cells (cell A and cell B), specially constructed by Dr. Happer's group at Princeton University. The cells were spheres of about 1 cm diameter Corning 7740 Pyrex glass that had been internally coated with Surfasil. The cells contained approximately 90% natural-abundance Xe (26.4% ^{129}Xe) and a few milligrams of Rb metal, with the remaining 10% composed of nitrogen. The internal pressure was 790 and 896 Torr for cells A and B, respectively.

Laser Polarization

The ^{129}Xe in the cells was routinely polarized at the Armstrong Laboratory of the Brooks Air Force Base at San Antonio using a tunable titanium:sapphire laser that was pumped by an argon laser. This laser system and optics delivered circularly polarized light between 1.6 and 1.7 W power at 795 nm to the wall of the chamber which contained the ^{129}Xe cells.

The cells were heated to 80°C in an oven to increase the Rb vapor density so that a substantial fraction of laser light could be absorbed. The aligning magnetic field of 27 G was provided by a set of Helmholtz coils. The heating chamber was constructed with optical windows for passage of the laser beam to the cell and an optical window port at 90° so that the fluorescence of the excited Rb, after passing through a cutoff filter to remove any 795 nm light, could be collected by a video camera and displayed. We found this to be a convenient way to periodically adjust the tuning of the laser to keep it on resonance. Typical polarization times were 25–30 minutes for each cell, which would result in a nuclear polarization level of ^{129}Xe of 5–20%. For these initial experiments, we had no device to determine the extent of polarization prior to freezing the ^{129}Xe for transport; however, our measurements did not rely on the knowledge of the exact magnitude of the initial hyperpolarization.

After 20–30 minutes of laser excitation and polarization, the cell was removed from the polarization chamber and frozen in liquid nitrogen in the presence of a magnetic field of about 50 G to lengthen the T_1 relaxation time of hyperpolarized Xe (*19*) for cross-town transport and further experimentation. A transportation system, composed of a liquid-nitrogen dewar and a permanent magnet aligned so as to produce a field parallel to the fringe field of our GE/Bruker 2 T/45 cm bore chemical-shift imager (CSI), was constructed to transport cells containing hyperpolarized ^{129}Xe from the Armstrong Laboratory to the Research Imaging Center (RIC) at the University of Texas Health Science Center, approximately a 30 min drive. Once the cells arrived at the RIC, the transportation device containing the cells was placed in the fringe field of the CSI to reduce the polarization loss. One cell was removed from the holding device and quickly transferred to the magnet bore, where it was rapidly thawed to room temperature in a beaker full of warm water. The cell was then placed in the ^{129}Xe RF coil (2.5 cm diameter, resonance frequency = 23.672668 MHz at 2 T) for further experiments.

T_1 Experiments

The T_1 measurements were made on a 2 T GE/Bruker 45 cm bore CSI and a 7.05 T GE/Bruker GN-300 89 mm bore spectrometer, at 20 and 22°C, respectively. On the CSI, a homebuilt ^{129}Xe RF coil was used; the GE/GN-300 on the other hand could be tuned to ^{129}Xe resonance frequency ($f = 83.0086234$ MHz). On each instrument, measurements were made using both methods (a) and (b). The RF pulse width–tip angle calibration depended only on the loaded quality factor of the resonator and the RF power level. For the same magnetic field, both cells had the same calibration factor but different T_1 (see Results).

Diffusion Experiments

All diffusion experiments were performed on the 2 T CSI scanner using the homebuilt ^{129}Xe RF coil. Once the RF pulsewidth–tip angle calibration was known, the next step in designing a diffusion experiment was to determine the required tip angles for the successive RF pulses, so that after each pulse, in the absence of any external gradients, the signal remained constant (Eq. [11]). For the six-pulse sequence (Fig. 1), the tip angles and the corresponding pulse widths are shown in Table 1. The next step was to optimize the experimental parameters: gradient strengths, g_n, gradient durations, τ_n, and the pulse repetition time, TR. We kept the gradient duration constant at $\tau = 9$ ms, and increased the gradient strength after each successive RF pulse so as

TABLE 1
RF Tip Angles and Corresponding Pulse Widths That Produce a Constant Signal in the Absence of Gradients (Eq. [11])

Rf pulse, n	Tip angle, θ (°)	Pulse width (μs)	Gradient, g_n (G/cm)	b_n (s/cm^2)
1	24.1	29.27	0	0
2	26.6	32.30	0.401	4.3
3	30.0	36.43	0.567	8.6
4	35.3	42.87	0.695	12.9
5	45.0	54.65	0.802	17.2
6	90.0	109.3	0.897	21.5

Note. The last two columns show the gradients used for a six-pulse diffusion experiment and the corresponding b_n (defined after Eq. [12]).

to keep the parameter b_n (defined after Eq. [12]) linear with n, the number of RF pulses (Table 1). The scan width was $\pm$1000 Hz, FID resolution was 2048 points, and the resulting acquisition time was 512 ms. A minimum TR = 884 ms was used.

RESULTS

RF Tip Angle Calibration

For both of the cells used in this study, the RF-coil loading was identical. RF pulse width–tip angle calibration was done several times during our studies using both methods (a) and (b), and the results were always consistent. For the calibration, we set TR $\ll T_1$, but TR $\geq T_2^*$ + acquisition time. The FID decay constant, T_2^*, varied from 15 to 30 ms. Since T_2^* depends on experimental conditions, e.g., shimming, it can vary over a wide range. Since acquisition time was 512 ms, and T_1 for ^{129}Xe was expected to be several minutes, TR was set to be about 1 s for our calibration and diffusion experiments. At a power level of 53dB, the 90° pulse had a pulse width of 109 $\pm$ 5 μs for both cells in the 2 T/CSI imaging system. For the 7.05 T/GE GN-300 spectrometer, the 90° pulse had a pulse width of 29 $\pm$ 3 μs at an RF power level of 62 dB. These values are the mean values of several measurements, and errors are simply the scatter in these measurements.

T_1 Measurements

The results of T_1 are shown in Table 2. The errors indicated are just the scatter in our measurements. For cell A at 2.0 T, measurements were made using both methods (a) and (b). Interpulse separation, TR, of 20, 30, 150, and 165 min and RF tip angles of 10° and 20° were employed. The T_1 values from all the measurements for cell A at different TR, different tip angle, and for both methods were found to be 155 $\pm$ 5 min. At 7.05 T, measurements on cell A were made using method (b), and measurements on cell B were made using method (a). A TR = 60 and 120 min, θ = 15° for cell A and TR = 60 min, θ = 15°, for cell B were used.

TABLE 2
T_1 Values for the Cells A and B at Two Magnetic Fields

Cell	2.0 T (20°C)	7.05 T (22°C)
A (790 Torr)	155 $\pm$ 5 min	185 $\pm$ 10 min
B (896 Torr)	66 $\pm$ 2 min	88 $\pm$ 5 min

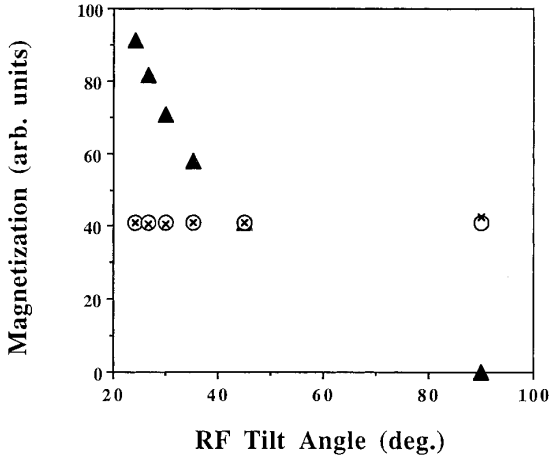

FIG. 2. Choice of RF tip angles to obtain constant signal in the absence of external gradients and no T_1 losses for a six-pulse sequence (Eq. [11]). The solid triangles, ▲, show the theoretical loss of hyperpolarized longitudinal magnetization as a result of successive RF tip angles (Eq. [1]). The circles, ○, show predicted signal values corresponding to the tip angles calculated from theory (Eq. [2]). The crosses, ×, show the experimentally measured signal values after successive RF pulses, for cell A. As can be seen, there is near-perfect match between the predicted signal values (○) and the experimentally measured (×) values. The RF tip angles used for these calculations and subsequent measurements are listed in Table 1.

Diffusion Results

For a six-pulse diffusion experiment, the experimental parameters are given in Table 1. Figure 2 shows the signal after each RF pulse predicted from Eq. [2] compared to the corresponding experimentally measured signal. As is clear from Fig. 2, an excellent agreement between the theoretically predicted signal and the experimentally measured signal is obtained and the desired effect of constant signal with successive pulses has been achieved. Figure 2 also shows the loss of hyperpolarized magnetization as a function of the RF tip angle. Note that for the last pulse, corresponding to a tip angle of 90°, the hyperpolarized magnetization has gone to zero; beyond this, there is no signal, and all the hyperpolarized magnetization has been effectively utilized.

Three sets of experiments were performed on each cell to determine the ^{129}Xe self-diffusion for each cell. In cell A, the data from the third diffusion experiment were very noisy due to a weak initial polarization and were excluded from

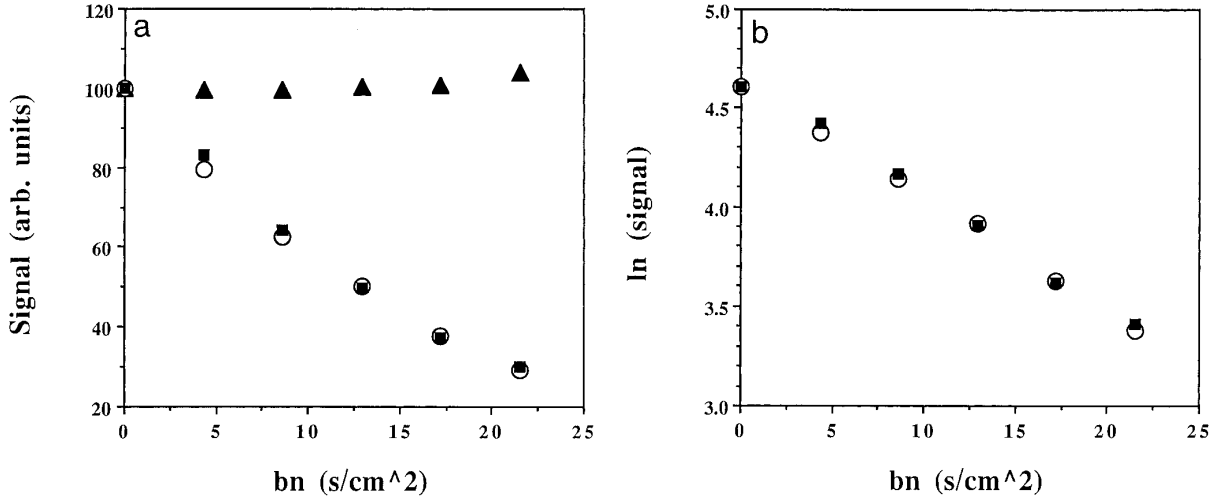

FIG. 3. (a) Signal in the presence of external gradients for the cell A as a function of the parameter, b_n, where b_n is defined after Eq. [12]. The b_n values are calculated from the gradient values, g_n. The values are listed in Table 1. The circles, ○, and the squares, ■, show experimental diffusion signal corresponding to two different experiments. Just for reference, the top flat part of the plot (▲) shows the signal corresponding to various tip angles in the absence of any external gradients. (b) The diffusion signal for two experiments plotted as a ln(signal) plot.

further calculations. The data for diffusion measurements are shown in Fig. 3 for cell A. Figure 3a shows the constant signal after successive RF pulses in the absence of the external gradients and also the exponentially decaying signal in the presence of the gradients. Figure 3b shows the natural log of the signal plotted as a function of b_n. As shown, the data are highly reproducible. The data from cell B were of comparable quality. The diffusion constant for ^{129}Xe self-diffusion was obtained by performing a linear regression on the $\ln(S_n/S_0)$ versus b_n data (Eq. [13]), and the results are shown in Table 3.

DISCUSSION

In this paper, we have introduced and successfully implemented methods to measure T_1 and self-diffusion of hyperpolarized ^{129}Xe. These methods take advantage of magnetic resonance of hyperpolarized ^{129}Xe nuclei.

In these methods, both T_1 and diffusion measurements depend on the accurate RF pulse width–tip angle calibration. We determined this calibration using both methods (a) and (b) discussed earlier. Method (a) has the advantage that the calibration is independent of the T_1 loss (Eq. [6]); however, it has the disadvantage that small errors in signal measurements I_1, I_2, and I_3 in Eq. [6], and subsequent solving of cubic equation in cos θ, propagate into larger errors in θ. Method (b) is simpler, since cos θ, rather than solving a cubic equation in cos θ, is directly calculated from the ratios of signals after adjacent RF pulses. Also, each n-pulse experiment gives $n - 1$ measurements of θ, yielding a more reliable measure of θ. The method assumes that TR $\ll T_1$ (Eq. [7]). This assumption is well satisfied in our experiments on the gas phase ^{129}Xe. In fact, this assumption will most likely be satisfied in most *in vivo* and *in vitro* studies because in this new magnetic resonance scheme, we do not have to wait for longitudinal magnetization to return to thermal equilibrium; consequently, TR is limited only by T_2^* and the data-acquisition time of the computer. So as long as T_1 is about 5 s [Ref. (*3*)] or more, the assumption that TR $\ll T_1$ can still be satisfied by using shorter TR. A good strategy for an accurate RF pulse width–tip angle calibration is to use pulse widths large enough to give tip angles in the range of 15–30°. At very small angles, small errors in cos θ can lead to large errors in θ. On the other hand, at larger angles, cos θ loss of hyperpolarized magnetization is substantial and the signal will reduce to the noise level after only a few RF pulses.

Once an accurate knowledge of RF pulse width–tip angle calibration is obtained, method (a) or (b) can be used to determine T_1. For T_1 measurements, there is no advantage in using method (a), so method (b) should be preferred to

TABLE 3
Results of Xe Self-Diffusion Measurements for the Two Cells

	Diffusion constant, D (cm^2/s)	
Experiment	Cell A (790 Torr, 20°C)	Cell B (896 Torr, 20°C)
1	0.057	0.041
2	0.058	0.045
3	—[a]	0.047

[a] Weak initial polarization, data unreliable.

minimize the errors and a TR $\approx T_1$ should be used. As shown in Table 2, both cells have quite different T_1 values. The T_1 relaxation is very sensitive to the spin environment. In the absence of any paramagnetic species (O_2, Rb, etc.), the dominant relaxation pathway will be through interactions with the cell walls. The differences in T_1 values for both cells at the same magnetic field can be attributed mostly to the differences in the cell wall structure at the microscopic and macroscopic level (*20*). As expected, the T_1 values increase with increasing magnetic field strength, because at the higher field, the spins precess at a higher frequency, so at the same temperature and pressure, fewer lattice atoms (wall atoms, N_2, etc.) vibrate at frequencies closer to the higher precession frequency, resulting in less favorable energy acceptance by the lattice from the spin system.

The diffusion measurements employ the pulse width (tip angle) optimization for successive RF pulses such that in an *N*-pulse experiment, the signal after each pulse, in the absence of external gradients, remains constant. Here again we make sure that TR $\ll T_1$, so that between successive RF pulses, the T_1 loss of hyperpolarized magnetization is negligible. Under these conditions, the only loss of hyperpolarized magnetization is the cos θ loss due to the RF tip angle, θ. However, θ can be increased to ensure that the signal loss due to cos θ loss of hyperpolarized magnetization is compensated by an increase in the tip angles of the successive pulses. The result of this formalism is given by Eq. [11]. In Fig. 2, the flatness of the predicted signal after each RF pulse confirms the accuracy of our choice of RF tip angles as well as confirming the accuracy of our RF pulse width–tip angle calibration. In addition, the robustness of our assumption that the T_1 loss of hyperpolarized magnetization between successive pulses is indeed negligible is vindicated.

The results of diffusion measurements for both cells are given in Table 3. As can be seen from Table 3, the values of D for each cell are very consistent between successive experiments. The D values for cell A are higher than the D values for cell B. This difference can in part be explained in terms of the higher pressure in cell B. Also the D value for cell A, 0.0575 cm^2/s, in which ^{129}Xe is at a pressure closer to the atmospheric pressure, is in excellent agreement with the D value for ^{129}Xe at 1 amagat, 0.051 cm^2/s (1 amagat = density of an ideal gas at 0°C and 1 atm, or 760 Torr pressure) obtained from theoretical extrapolation of high pressure D values for ^{129}Xe (*13*). Recently, D values for ^{129}Xe using laser-polarized ^{129}Xe NMR have been reported (*14*). That method involved the determination of the spatial distribution of the RF pulse profile, $B_1(z)$, and employed several assumptions and a fairly complicated model for the diffusion of longitudinal magnetization. A value of 0.16 ± 0.04 cm^2/s at 150 Torr and 300 K for ^{129}Xe self-diffusion, compared to 0.26 cm^2/s obtained from theoretical extrapolation of high-pressure experimental data, was obtained. The method described in this paper is simpler and the agreement with the theoretically extrapolated values from high pressure data much better. It requires fewer assumptions, which can more easily be satisfied by the design of the experiment, and the validity of these assumptions can be internally checked (constant signals after successive RF pulses Fig. 2).

The methods introduced in this paper are in principle applicable for T_1 and diffusion measurements *in vivo* using hyperpolarized ^{129}Xe magnetic resonance. If *in vivo*, TR $\ll T_1$, and TR $\sim T_2^*$, leftover transverse magnetization may lead to unwanted echos. In that case, spoiler gradients may be employed. These methods are theoretically sound and simple to implement. With growing interest in the potential applications of hyperpolarized ^{129}Xe magnetic resonance in imaging of human lungs, brain, and blood flow, there are two very important questions that must be answered: (i) how much, if any, hyperpolarized magnetization will survive by the time the hyperpolarized Xe reaches the target tissue (e.g., brain) and (ii) how fast Xe will diffuse/perfuse into the tissue in the target organ. The methods presented in this paper can be useful in answering these questions.

ACKNOWLEDGMENT

The authors express their sincere thanks to Professor William Happer, Princeton University, for his help.

REFERENCES

1. M. S. Albert, G. D. Cates, B. Driehuys, W. Happer, B. Saam, C. S. Springer Jr., and A. Wishnia, *Nature* **370,** 199–201 (1994).
2. H. Middleton, R. D. Black, B. Saam, G. D. Cates, G. P. Cofer, R. Guenther, W. Happer, L. W. Hedlund, G. A. Johnson, K. Juvan, and J. Swartz, *Magn. Reson. Med.* **33,** 271–275 (1995).
3. M. S. Albert, V. D. Schepkin, and T. F. Budinger, *J. Comput. Assist. Tomogr.* **19,** 975–978 (1995).
4. N. D. Bhaskar, W. Happer, and T. McClelland, *Phys. Rev. Lett.* **49,** 25–28 (1982).
5. W. Happer, E. Miron, S. Schaefer, D. Schreiber, W. A. van Wijngaarden, and X. Zeng, *Phys. Rev. A* **29,** 3092–3110 (1984).
6. G. D. Cates, R. J. Fitzgerald, A. S. Barton, P. Bogard, M. Gatzke, N. R. Newburry, and B. Saam, *Phys. Rev. A* **65,** 4631–4639 (1992).
7. M. S. Albert, C. S. Springer, and A. Wishnia, Abstracts of the Society of Magnetic Resonance in Medicine, 11th Annual Meeting, New York, p. 2104, 1992.
8. M. S. Albert, C. S. Springer, and A. Wishnia, Abstracts of the Society of Magnetic Resonance in Medicine, 11th annual meeting New York, p. 4710, 1992.
9. M. S. Albert, D. Balamore, K. Sakai, D. Kacher, R. L. Walsworth, E. Oteiza, and F. A. Jolesz, Abstracts of the Society of Magnetic Resonance, 4th Annual Meeting, p. 1357, 1996.
10. M. E. Wagshul, T. M. Button, H. F. Li, Z. Liang, C. S. Springer, K. Zhong, and A. Whishnia, *Magn. Reson. Med.* **36,** 183–191 (1996).
11. M. S. Albert, C. H. Tseng, D. Williamson, E. R. Oteiza, R. L. Walsworth, B. Kraft, D. Kacher, B. L. Holman, and F. A. Jolesez, *J. Magn. Reson. B* **111,** 204–207 (1996).
12. K. Sakai, A. M. Bilek, E. R. Oteiza, R. L. Walsworth, D. Balamore,

F. A. Jolesez, and M. S. Albert, *J. Magn. Reson. B* **111,** 300–304 (1996).

13. P. W. E. Peereboom, H. Luigjes, and K. O. Prins, *Physica A* **156,** 260–276 (1989).
14. G. R. Davies, T. K. Halstead, R. C. Greenhow, and K. J. Packer, *Chem. Phys. Lett.* **230,** 237–242 (1994).
15. J. H. Gao, L. Lemen, J. Xiong, B. R. Patyal, and P. T. Fox, *Magn. Reson. Med.* **37,** 153–158 (1997).
16. M. K. Stehling, *Mag. Reson. Imaging* **10,** 165–167 (1992).
17. L. Zhao, R. Mulkern, C. H. Tseng, D. Williamson, S. Patz, R. Kraft, R. L. Walsworth, F. A. Jolesz, and M. S. Albert, *J. Magn. Reson. B* **113,** 179–183 (1996).
18. E. O. Stejskal, and J. E. Tanner, *J. Chem. Phys.* **42,** 288–292 (1965).
19. M. Gatze, G. D. Cates, B. Driehuys, D. Fox, W. Happer, and B. Saam, *Phys. Rev. Lett.* **70,** 690–693 (1993).
20. B. Driehuys, G. D. Cates, and W. Happer, *Phys. Rev. Lett.* **74,** 4943–4946 (1995).